

The Timescale, Power Spectra, and Climate Noise Properties of Teleconnection Patterns

STEVEN B. FELDSTEIN

Earth System Science Center, The Pennsylvania State University, University Park, Pennsylvania

(Manuscript received 20 August 1999, in final form 31 January 2000)

ABSTRACT

This study uses NCEP–NCAR reanalysis data covering the boreal winters of 1958–97 to examine the power spectral, timescale, and climate noise properties of the dominant atmospheric teleconnection patterns. The patterns examined include the North Atlantic oscillation (NAO), the Pacific–North American (PNA), and west Pacific (WP) teleconnections, and a spatial pattern associated with ENSO. The teleconnection patterns are identified by applying a rotated principal component analysis to the daily unfiltered 300-mb geopotential height field. The NAO and PNA were found to be the two dominant patterns on all timescales.

The main finding is that the temporal evolution of the NAO, PNA, and WP teleconnections can be interpreted as being a stochastic (Markov) process with an e -folding timescale between 7.4 and 9.5 days. The time series corresponding to the ENSO spatial pattern did not match that of a Markov process, and thus a well-defined timescale could not be specified. The shortness of the above timescales indicates that the excitation of these teleconnection patterns is limited to a period of time less than a few days. These findings also suggest that in order to improve our understanding of the growth and decay mechanisms of teleconnection patterns, it is best to use daily, unfiltered data, rather than monthly or seasonally averaged data.

The signal (interannual variance due to external forcing) to noise (interannual variance from stochastic processes) ratios were also examined. For the NAO (PNA), the signal-to-noise ratio is 0.09 (1.11). This indicates that the interannual variability of the NAO (PNA) arises primarily from climate noise (both from climate noise and external forcing). An explanation for why the NAO and PNA dominate on interannual timescales is also presented.

1. Introduction

Most investigations of the properties of low-frequency anomalies, such as the North Atlantic oscillation (NAO) and Pacific–North American (PNA) teleconnection patterns, use either monthly or seasonally averaged data (e.g., Wallace and Gutzler 1981; Barnston and Livezey 1987). Although there are valuable benefits to using such time-averaged data, especially from the perspective of long range forecasting, such time averaging could obscure some of the underlying dynamical processes if the timescale of these anomalies is much shorter than 2 months. A hint that the timescale for a number of low-frequency anomalies may indeed be much less than 1 month can be found in the investigation of persistent anomalies by Dole (1986), where it was found that persistent anomalies over the North Pacific, North Atlantic, and Siberia all decay with an “integral timescale” (Leith 1973) on the order of 15 days.

In this study, we examine the timescale of low-frequency anomalies with the aid of power spectrum analysis. Each of the anomalies is identified through the application of a rotated principal component analysis (RPCA) to the daily unfiltered 300-mb geopotential height field, and the spectral analysis is applied to each principal component (PC) time series. As will be shown, several of the prominent low-frequency anomalies are well described as a Markov process (also known as a red noise or first-order autoregressive process). A Markov process satisfies the equation (e.g., Chatfield 1989)

$$x_t = \alpha x_{t-1} + F_t, \quad (1)$$

where x_t is, say, one of the PC time series on the t th day, F_t is Gaussian white noise forcing, and α is a positive constant with a value less than unity. If the PC time series can be described by (1), then it tells us that the forcing that drives the anomaly can be modeled as being stochastic, and that the amplitude of the anomaly decays by a factor of e in $T = -1/\ln\alpha$ days. As we will see, for all of the dominant atmospheric low-frequency anomalies, this e -folding timescale T , which is the only relevant timescale for a Markov process, has a value between 6 and 10 days, which is obviously much less

Corresponding author address: Dr. Steven B. Feldstein, Earth System Science Center, The Pennsylvania State University, 0221 Deike Bldg., University Park, PA 16802.
E-mail: sbf@essc.psu.edu

than 2 months. The power spectral density function, $f(\omega)$ (e.g., Chatfield 1989), corresponding to (1) is

$$f(\omega) = \frac{\sigma_x^2(1 - \alpha^2)}{\pi(1 - 2\alpha \cos\omega + \alpha^2)}, \quad (2)$$

where ω is the frequency, and σ_x^2 the variance of the x_t time series. If the power spectrum takes on the form of (2) at most frequencies, except for one or more particular frequencies where $f(\omega)$ is substantially larger (as measured by a test of statistical significance) than at neighboring frequencies, then in addition to the Markov process with its e -folding timescale T , x_t can be said to be undergoing a cyclic process at the frequencies corresponding to the spectral peaks.

For those low-frequency anomalies that are well described as a Markov process, we will address the question of whether the interannual variability of these anomalies can be interpreted as arising from climate noise (e.g., Leith 1973; Madden 1976; Madden and Shea 1978; Trenberth 1984, 1985; Dole 1986; Feldstein and Robinson 1994). The question of climate noise can be framed within the perspective of whether the variance associated with interannual fluctuations of anomalies such as the NAO, PNA, or even El Niño–Southern Oscillation (ENSO), arises from statistical sampling fluctuations associated with the much shorter 6–10-day fluctuations of the same anomaly. Such interannual fluctuations are to be expected for any Markov process, no matter how short the timescale. If the amplitude of the interannual fluctuations, as measured by its variance, falls within the range of variability expected for a Markov process, then the interannual fluctuations can be entirely attributed to climate noise associated with unpredictable, much shorter timescale fluctuations. On the other hand, if the amplitude of the interannual fluctuations exceeds some particular climate noise threshold, then in addition to the always present climate noise contribution, these interannual fluctuations are also likely driven by some external process, such as interannual variations in sea surface temperature (SST; e.g., Horel and Wallace 1981; Mo and Livezey 1986; Zhang et al. 1996).

In section 2, the data and diagnostic techniques are described. The results of the RPCA calculations are shown in section 3. The findings of the spectral and climate noise analyses are presented in section 4, followed by a discussion and conclusions in section 5.

2. Data and diagnostic techniques

We use the daily unfiltered, 300-mb geopotential height field from the National Centers for Environmental Prediction–National Center for Atmospheric Research reanalysis dataset. The data analyzed extend from 1 January 1958 to 31 December 1997, and are restricted to the winter season, defined as the months of December–February. Also, the seasonal cycle is subtracted at each grid point. The seasonal cycle is obtained by cal-

culating the time mean geopotential height for each calendar day followed by smoothing with a 20-day low pass digital filter. From the daily data, two additional datasets are generated, one consisting of monthly averages and the other of seasonal averages. The anomaly spatial structures, that is, rotated empirical orthogonal functions (REOFs), and the corresponding orthonormal PC time series, are obtained by applying a RPCA with a varimax rotation to each of the three datasets. For these calculations, the eigenvectors of the covariance matrix are calculated. The issues discussed in the introduction are then addressed by examining power spectra, lagged autocorrelations, and χ^2 statistics of the corresponding PC time series. Also, the PC time series will be compared to the time series of various teleconnection pattern and tropical Pacific SST indices made available by the Climate Prediction Center (CPC). These teleconnection indices are based on the methodology of Barnston and Livezey (1987; BL, hereafter).

3. Daily, monthly, and seasonal-averaged REOFs

We begin by examining the first four REOFs of the seasonally averaged 300-mb geopotential height field (Fig. 1), and then show that extremely similar REOF patterns are present in the monthly averaged and daily (0000 UTC) time series (Figs. 2 and 3, respectively). Each frame indicates the ranking and the corresponding fractional variance. For these calculations, eight unrotated EOFs were retained. Both the spatial patterns and the corresponding PC time series were found to be rather insensitive to the number of retained unrotated EOFs, when tested over a range of between 6 and 15 unrotated EOFs. As is typical of RPCA, for larger numbers of retained unrotated EOFs, the patterns became increasingly localized.

a. Similarities in spatial structure

Figures 1, 2, and 3 show that extremely similar REOFs do indeed occur in the seasonally averaged, monthly averaged, and daily data. Furthermore, these spatial patterns closely resemble those presented in BL. For example, a pattern resembling the NAO (a dipole in the North Atlantic with one center over Greenland and the other in midlatitudes) is clearly evident as REOF1 in Figs. 1, 2, and 3. Similarly, a pattern resembling the PNA (a quadrupole with centers over the subtropical Pacific near Hawaii, south of the Aleutian Islands, northwestern Canada, and the southeastern United States), appears as REOF2 in Figs. 1, 2, and 3. (The features of both the NAO and PNA are discussed in detail by BL.) The REOF3 pattern in the seasonally averaged data (Fig. 1c) is also present in the monthly averaged and daily data (Figs. 2c and 3c). However, in the latter two datasets, this particular pattern is found to compose a much smaller fraction of the variance. In fact, this pattern, which we will refer to as the “at-

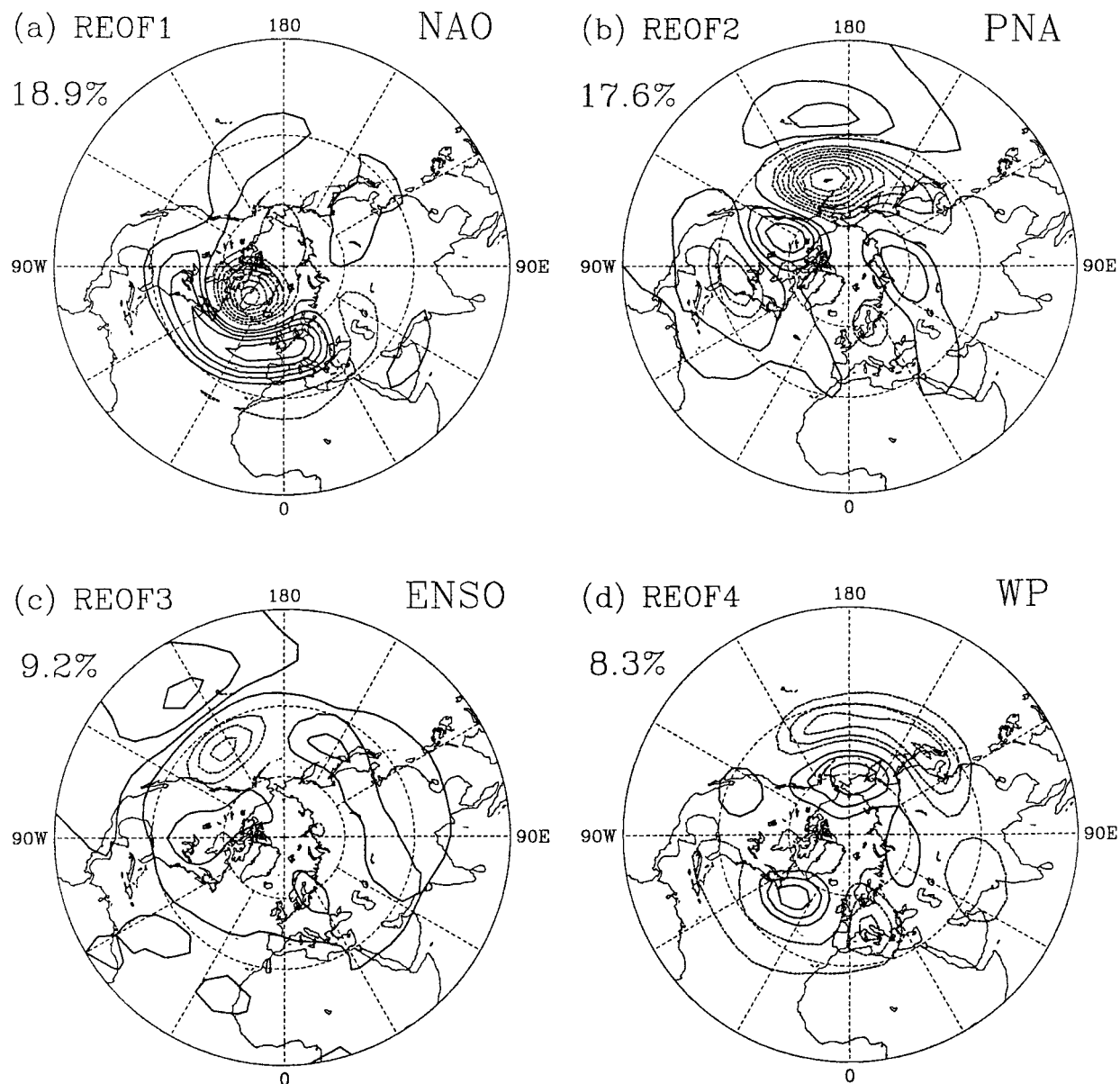


FIG. 1. The seasonally averaged REOFs. The name, ranking, and fractional variance of each REOF is shown. The contour interval is the same for each frame. Solid contours are positive, dashed contours negative, and the zero contour is omitted.

mospheric ENSO" pattern, is not present with eight REOFs in the monthly averaged and daily data, and can be obtained only if the number of REOFs is increased to 10 and 20, respectively. The REOF4 pattern in Fig. 1, which is characterized by a dipole structure in the North Pacific, resembles the west Pacific oscillation (WPO) pattern of BL. Furthermore, this pattern is also similar to REOF3 and REOF6 of the monthly averaged and daily data, respectively. Additional patterns in BL, such as EU1, EA, EU2, and EP are also present in the daily, monthly, and seasonal data. (It should be noted that the CPC refers to the EU1, EU2, and WPO patterns as the SCA, EA/WR, and WP patterns, respectively.)

However, since these patterns are less prominent, they are not illustrated, and their timescale and climate noise properties will be briefly summarized in the conclusions.

b. Temporal correlations

In addition to noting the above similarities between various REOF spatial patterns and those of BL, an objective comparison is made by calculating the linear correlation between each of the monthly averaged PC time series and the corresponding CPC teleconnection pattern index time series. The resulting linear correlations are found to have values of 0.76, 0.86, and 0.66,

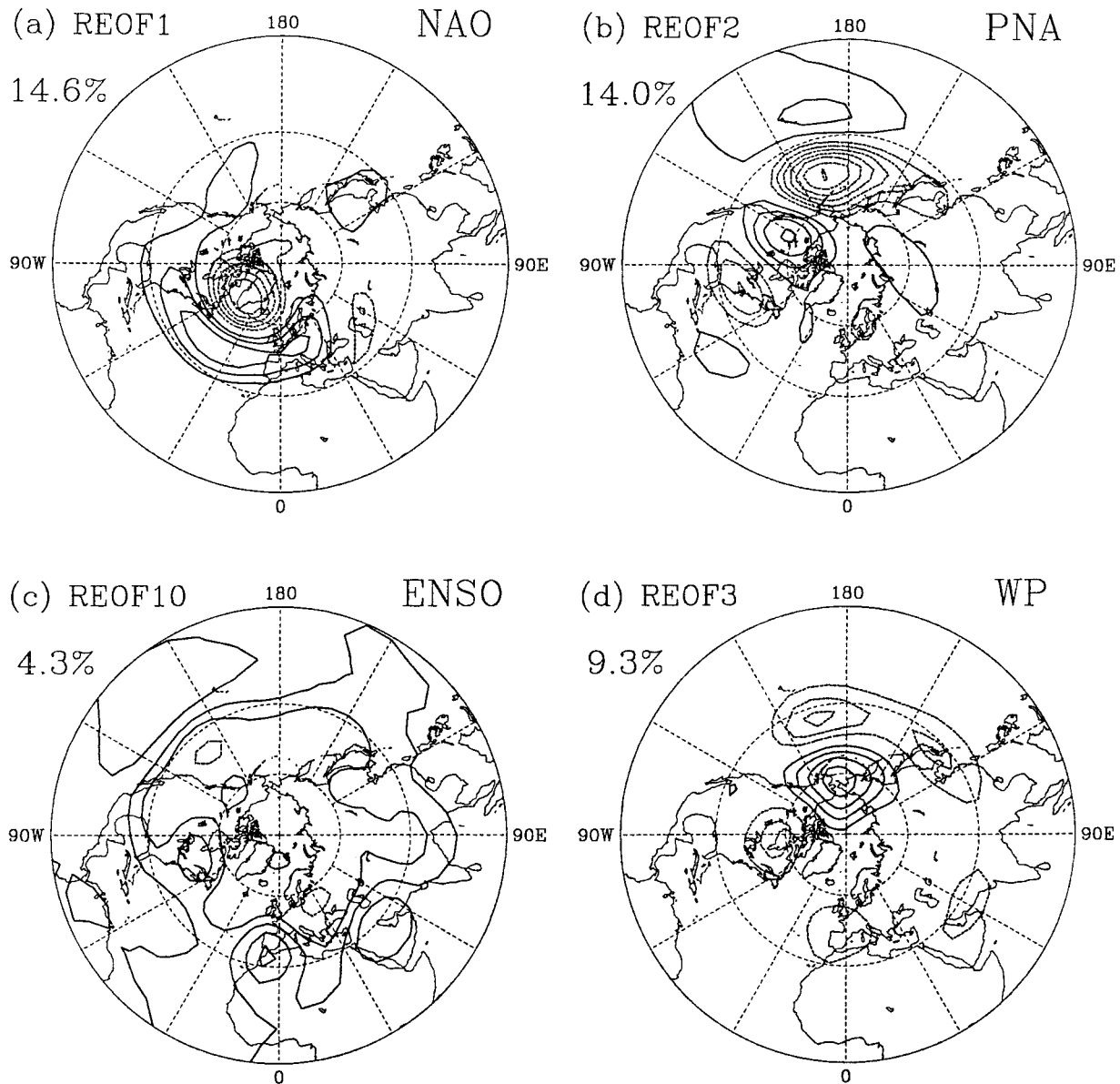


FIG. 2. As in Fig. 1 except for monthly averaged data.

for the NAO, PNA, and west Pacific (WP) patterns, respectively. All of these correlations are in excess of the 99% confidence level. The large values for these correlations are indeed reassuring, especially when one notes that the CPC teleconnection index is derived from data on a different pressure surface; that is, BL use the 700-mb level, calculate the eigenvectors from a correlation matrix, and apply the RPCA to individual calendar months, rather than to a time series of consecutive months as in this study. Thus, one can be confident that the REOFs in Fig. 2 do correspond to those particular patterns found by BL. These same patterns are also obtained in numerous other studies of low-frequency variability (see BL for references).

The PC time series of the REOF10 pattern in Fig. 2, was not related to any of the CPC teleconnection indices. An inspection of the spatial structure of REOF10 suggests that it may be related to the TNH pattern of BL. However, the linear correlation between the PC time series associated with REOF10 and the TNH index time series yielded a value of only 0.21. On the other hand, the PC time series of REOF10 was found to be highly correlated to the various eastern tropical Pacific SST indices of NOAA which cover the following regions; Niño-3 (5°N – 5°S , 150° – 90°W), Niño-3.4 (5°N – 5°S , 170° – 120°W), and Niño-4 (5°N – 5°S , 160°E – 150°W). For example, the monthly PC10 was linearly correlated with the Niño-3, Niño-3.4, and Niño-4 indices at a value

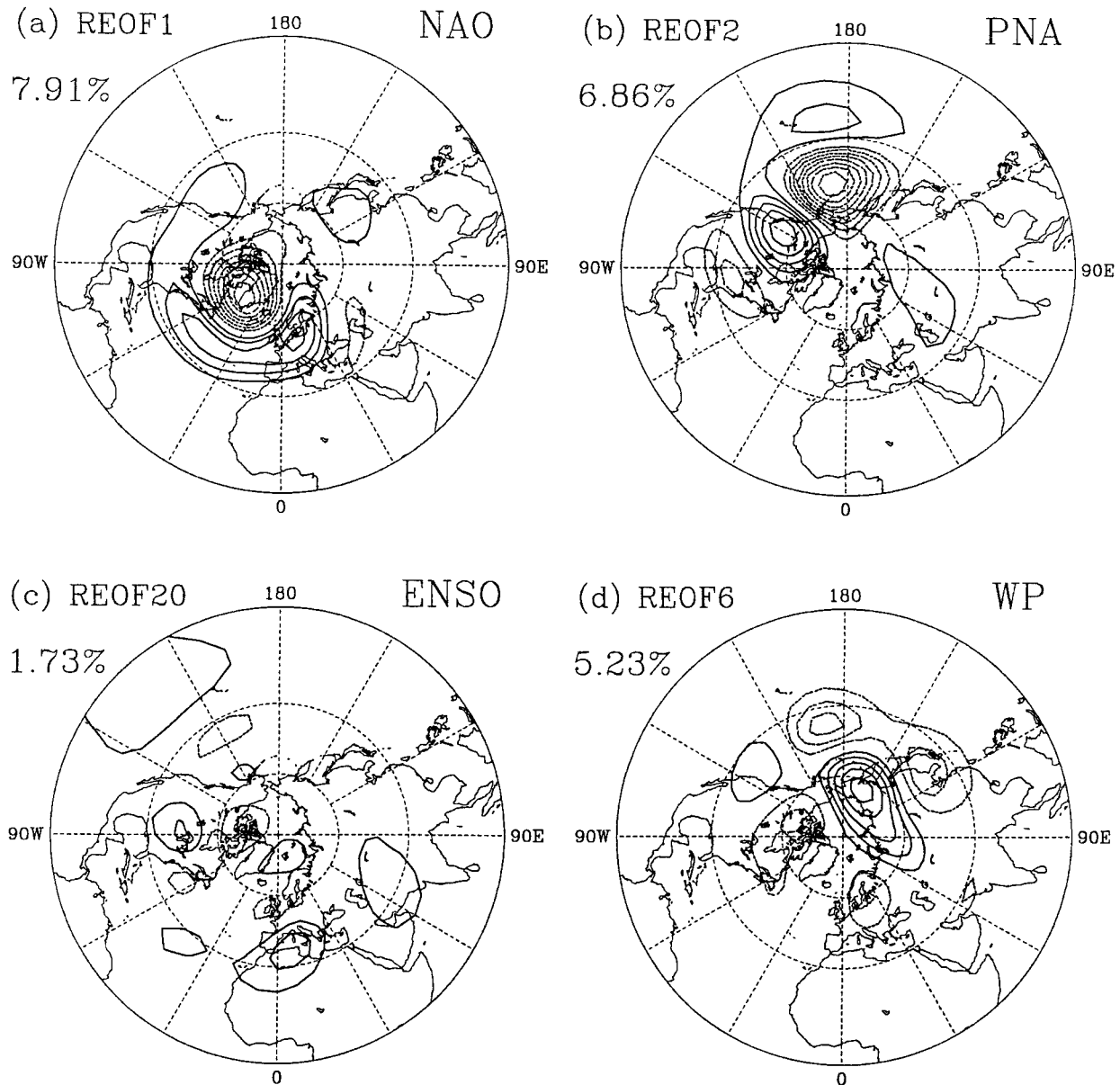


FIG. 3. As in Fig. 1 except for daily unfiltered data.

of 0.60, 0.63, and 0.67, respectively. Further support for a fairly strong relationship between this particular spatial pattern and the tropical Pacific SST field can be seen by linearly correlating the seasonal mean PC3 with the seasonal mean Niño-3, Niño-3.4, and Niño-4 indices. This calculation yielded values of 0.66, 0.70, and 0.79, respectively. As these tropical SST indices are commonly used to represent ENSO, this finding establishes a link with the monthly REOF10 and the seasonal REOF3 to ENSO, and also motivates our use of the terminology “atmospheric ENSO” pattern.

A higher linear correlation is obtained when the tropical SST indices are correlated with the predictand of a multiple regression equation in which the Niño-3.4 in-

dex is regressed onto the atmospheric ENSO, PNA, and WP PC time series. With this choice of independent variables in the multiple regression equation, for interannual timescales, the linear correlation between the predictand and the Niño-3.4 index was found to have a value of 0.84. Application of analysis of variance shows that this linear correlation exceeds the 99% confidence level. The coefficients in the regression equation are 10.5, 3.3, and -2.0 , for the atmospheric ENSO, PNA, and WP PC time series, respectively. This suggests that although each of the PC time series is uncorrelated, these PC time series tend to come into phase with each other during ENSO events. As a result, the atmospheric response to ENSO SST anomalies mostly involves a

TABLE 1. Linear correlations among daily (d), monthly (m), and seasonal (s) PC.

	d vs m	d vs s	m vs s
NAO	0.97	0.98	0.96
PNA	0.95	0.97	0.96
Atmospheric ENSO	0.82	0.80	0.77
WP	0.74	0.65	0.86

superposition of REOFs, with the atmospheric ENSO pattern making up the largest contribution.

Although the strong similarity between the daily and monthly REOF spatial patterns suggests that the daily REOF patterns can also be identified with particular BL anomaly patterns, or with the atmospheric ENSO pattern for the daily REOF20, we objectively evaluate these relationships by performing the following calculation. Take the daily PC time series and construct another time series consisting of nonoverlapping monthly averaged segments. This new time series is then correlated with the corresponding monthly averaged PC time series. As each pair of time series yields a large linear correlation (see Table 1), we are able to identify the daily REOF in Fig. 3 with a particular BL teleconnection pattern, and REOF20 with the atmospheric ENSO pattern.

The seasonally averaged REOFs (Fig. 1) are identified by an analogous procedure whereby a new time series consisting of nonoverlapping seasonally averaged segments of the monthly averaged PC time series is correlated with the seasonally averaged PC time series. Most of these correlations are very high, particularly the NAO and PNA (Table 1). Also, the daily and seasonally averaged PC time series are compared by following the same procedure in which nonoverlapping seasonally averaged segments of the daily PC time series are correlated with the seasonally averaged PC time series (Table 1). Again large correlations are found. This indicates that to a large extent the monthly and seasonally averaged PC can be simply interpreted as time averages of the corresponding daily PC time series. Furthermore, these results also indicate that the essential temporal information about these teleconnections is contained within the daily PC time series.

4. Power spectra, timescale, and climate noise

a. Power spectra

In order to evaluate the power spectra, timescale, and climate noise properties, it is best to use a daily, unfiltered, time series. Although one could use the daily PC time series from the previous section, we adopt the following approach for each teleconnection pattern. First, we take the monthly and seasonally averaged REOFs, and projected the daily (0000 UTC) 300-mb height fields onto these spatial patterns. This approach generates two new daily time series. Then, we compare the variance of these two time series with that from the

daily PC time series, and select the time series with the greatest variance. This approach finds that for the NAO and PNA the daily PC time series still retains the largest variance. On the other hand, for the atmospheric ENSO (WP) pattern, it is found that daily time series generated from the seasonally (monthly) averaged REOFs yields the largest variance.

We next examine the power spectra for the daily PC time series (see Fig. 4). These power spectra are displayed for two separate ranges of periods, referred to as intraseasonal (2–90 days) and interannual (2–20 yr). Before calculating these power spectra, all linear trends have been removed, and the ends of each time series were tapered. A comparison of the power spectra with and without the trend removal showed that the trend removal had a negligible influence on all spectra except for the NAO, which exhibited a very large trend on interannual timescales. The intraseasonal power spectra are obtained by calculating the average of individual power spectra for each of the 39 winter seasons. The interannual power spectra are derived by applying a Hanning window to the seasonally averaged daily PC time series. In addition to these smoothed power spectra, Fig. 4 also shows red noise spectra, and the 95% a priori and 95% a posteriori confidence levels. The shape of these red noise spectra, that is, the value of α in (2), were determined from a least squares fit to the smoothed intraseasonal power spectra in Fig. 4. The interannual red noise spectra were calculated by extending the intraseasonal red noise spectra toward interannual timescales. For determining the intraseasonal confidence limits, 78 degrees of freedom are used for each spectral estimate, where it has been assumed that there are approximately two degrees of freedom for each seasonal periodogram value. For the interannual power spectra, the number of degrees is $(2N - m/2)/m$, where N is the number of years, and m is the truncation point (see Panofsky and Brier 1968).

We first concentrate on the characteristics of the intraseasonal power spectra. For the NAO, PNA, and WP PC time series, the power spectrum does indeed resemble that for a Markov process. Furthermore, none of the power spectra for these three PC time series exhibit spectral peaks that exceed the 95% a posteriori confidence level. On the other hand, the power spectrum for the atmospheric ENSO PC shows a broad peak near 20 days that exceeds the 95% a posteriori confidence level. Consistently, calculations of the autocorrelation function (not shown) for the atmospheric ENSO PC indicate large deviations from that for a Markov process at lags beyond 10 days. For lags less than 10 days, the autocorrelation function decays at a rate matching that of a Markov process with a 20-day e -folding timescale. However, at larger lags, the autocorrelation function declines more slowly, not reaching e^{-1} until 49 days. This suggests that the atmospheric ENSO PC time series is not well described by a Markov process.

For the interannual power spectra, it is only the PNA

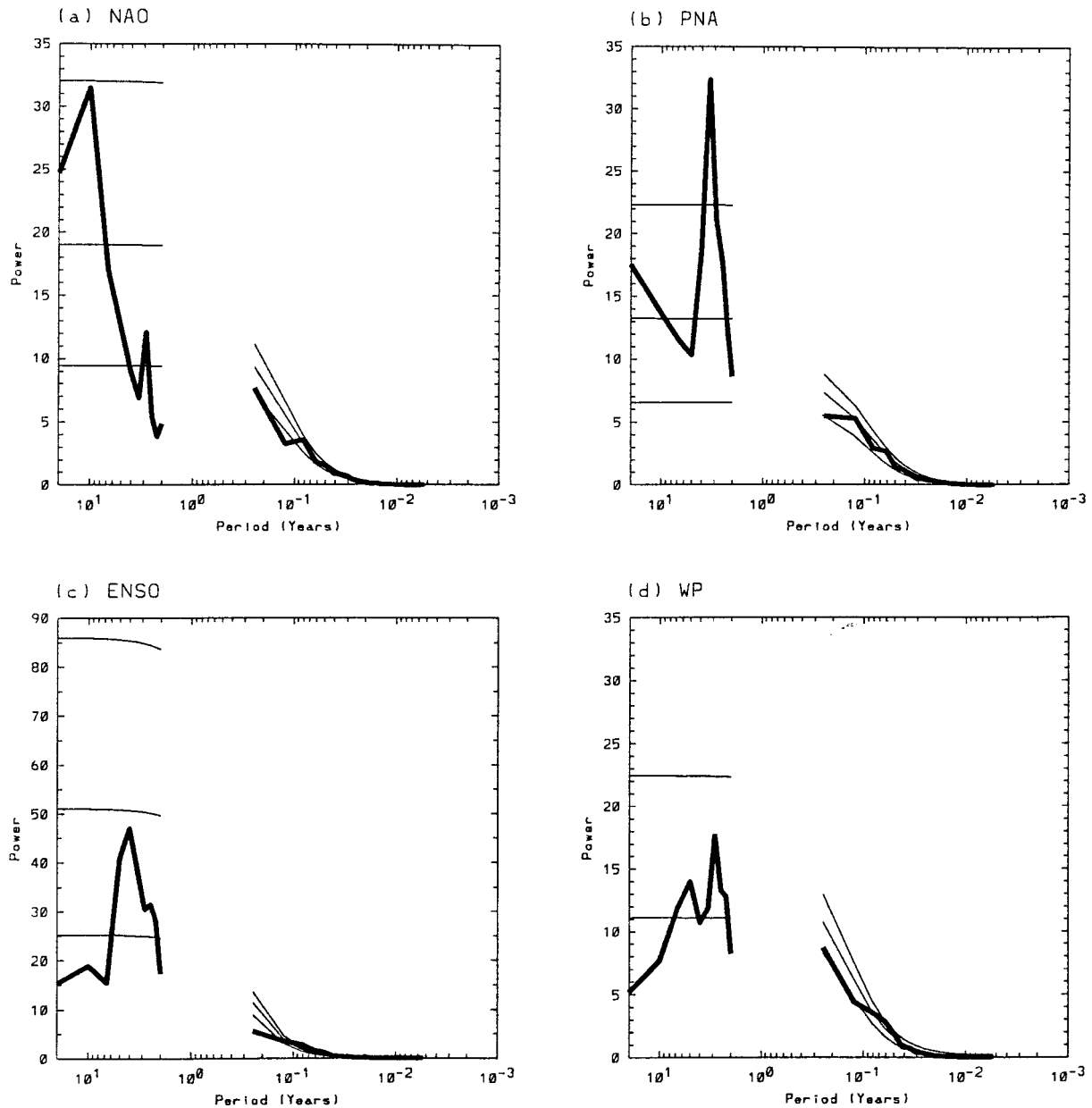


FIG. 4. Power spectra (thick lines) for the daily PC time series. The red noise spectra (lower thin lines) and 95% a priori (middle thin lines) and a posteriori (upper thin lines) confidence levels are also shown.

PC time series that exhibits a spectral estimate (near 4 yr) that is above the 95% a posteriori confidence level. The occurrence of this spectral peak in the PNA PC time series is certainly not surprising, as other studies have found that the PNA is related to ENSO (e.g., Mo and Livezey 1986), and numerous ENSO investigations find a spectral peak near 4 yr (e.g., Zhang et al. 1996; Kestin et al. 1998; Zhang et al. 1998; Wunsch 1999). The atmospheric ENSO PC also exhibits a spectral peak near 4 yr, but it fails to exceed the 95% a priori confidence level. When we compare the interannual atmospheric ENSO power spectrum with that for a white

noise process, the 4-yr peak also falls slightly below the 95% a priori confidence level.

b. Timescale

Given that the intraseasonal power spectra in Fig. 4 appear to be well represented by a Markov process (except for the atmospheric ENSO PC), we define a timescale for the NAO, PNA, and WP PC time series based on the time taken for the autocorrelation function of each PC time series to decrease by a factor of e . These e -folding timescales, shown in Table 2, reveal that each

TABLE 2. Timescale and χ^2 .

	Timescale (days)	χ^2
NAO	9.5	63.9
PNA	7.7	82.4
WP	7.4	44.8

PC time series has a timescale between 7.4 and 9.5 days. Such values, of course, correspond to frequencies much larger than the $1/(2 \text{ month})$ Nyquist frequency in many studies of low-frequency variability.

c. Climate noise

In this section, we address the question of whether the interannual variability of some anomalies can be interpreted as arising from climate noise. We follow the approach in Dole (1986) and Feldstein and Robinson (1994) to test for climate noise in each of the PC time series. This approach involves the examination of the statistical significance of $\chi^2 = NS_p^2/S^2$, which has $N - 1 = 38$ degrees of freedom, one less than the number of winter seasons in the dataset, where S_p^2 is the interannual variance of the daily unfiltered PC time series, and S^2 is the interannual variance of the Markov process represented by the corresponding intraseasonal red noise spectra in Fig. 4. (Because the atmospheric ENSO PC is not well represented by a Markov process, a climate noise analysis for this particular teleconnection pattern is not performed.) For the purpose of calculating S^2 , a 10 000-yr synthetically generated time series was obtained that has the same variance and lag 1 day autocorrelation as the corresponding PC time series. Our null hypothesis is that S_p^2 is not greater than S^2 , that is, $\chi^2 = N$, and the χ^2 threshold value corresponding to the 95% confidence level for a one-sided test is 53.4.

As shown in Table 2, the χ^2 values for the NAO and PNA PC time series are well in excess of the 95% confidence level. The χ^2 value for the WP pattern is well below this threshold, which suggests that the interannual fluctuations of this pattern can be entirely attributed to climate noise. Returning to the NAO and PNA PC time series, although climate noise contributes toward their interannual variability, the χ^2 values in Table 2 indicate that some amount of external forcing is also playing a key role. However, it is important to note that the occurrence of a χ^2 value that exceeds the 95% confidence level does not, per se, indicate that the interannual variability is dominated by the external forcing. Such a χ^2 value simply indicates that the interannual variability is greater than that expected for a Markov process, at least to the 95% confidence level. For the purpose of examining the relative importance of external forcing and climate noise, we will calculate the signal-to-noise ratio, a quantity that can be determined from χ^2 . Such an analysis will be presented later in this section.

Because the NAO exhibits a large linear trend over the 40 yr between 1958 and 1997, as indicated in section

4a, this teleconnection warrants further investigation. A calculation of χ^2 for the NAO with and without the trend reveals that most of the excess variance above the 95% confidence level is accounted for by the large linear trend. Since Hurrell and van Loon (1997) (HV hereafter) show that this trend does not extend to those years prior to 1958 (HV defined a winter mean NAO index based on sea level pressure, which allows them to evaluate the NAO back to 1864), and because the stochastically driven, synthetic NAO time series of Wunsch (1999) shows episodes with similar linear trends, it may be that the large interannual variance associated with the NAO, and hence the large χ^2 value, arises because we have sampled a particularly unusual 40-yr period. Or stated in other words, the sample size may simply be too small. To address this question, we use the NAO index time series of HV, which is obtained from NCAR, as a proxy measure for the PC time series associated with the NAO. The fact that the correlation between the HV NAO time series and our NAO time series is found to be 0.89 for the years of 1958–97 provides support for this approach. We then estimate the 1864–97 interannual variance of the NAO time series by assuming that the ratio of the 1864–97 variance to the 1958–97 variance is the same for both time series. Upon using this estimated value for the interannual variance of the NAO time series, a χ^2 value of 145.8 is obtained. Such a value falls slightly less than halfway between that for the null hypothesis, that is, $\chi^2 = N = 134$, and that for the corresponding 95% confidence level, which is 160.9 for 133 degrees of freedom. Thus, it is difficult to make a strong statement about the role of climate noise and external forcing for the NAO.

To investigate the relative roles of external forcing and climate noise for interannual variability, we next examine the signal-to-noise ratio. The signal is interpreted as resulting from external forcing, and is regarded as the amount that the observed interannual variance exceeds the interannual variance of the corresponding Markov process, that is, $S_p^2 - S^2$. Specifying the noise to be S^2 , the signal-to-noise ratio takes the simple form $\chi^2/N - 1$. A calculation of this quantity yields a signal-to-noise ratio of 0.09 and 1.11 for the NAO and PNA PC time series, respectively (for the NAO, the 134-yr estimate for χ^2 was used). For the NAO, this result indicates that most of the interannual variance of this pattern can be interpreted as arising from climate noise. On the other hand, climate noise accounts for about one-half of the interannual variance of the PNA.

5. Discussion and conclusions

In this study, the spectral, timescale, and climate noise characteristics of the dominant Northern Hemisphere winter teleconnection patterns are examined. These patterns are identified with RPCA as the NAO, PNA, and WP patterns of Barnston and Livezey (1987), and another pattern referred to as the atmospheric ENSO pat-

tern. The latter pattern was found to be closely related to the tropical SST anomalies associated with ENSO. The key finding of this study is that the temporal evolution of the NAO, PNA, and WP patterns can be interpreted as being a stochastic process with an e -folding timescale between 7.4 and 9.5 days. Similar stochastic properties were also found for other less prominent teleconnection patterns, such as the EA, EA/WR, and SCA patterns. The e -folding timescale associated with these patterns was typically between 6 and 7 days. On the other hand, a similar statement about stochastic properties for the atmospheric ENSO pattern could not be made, as its intraseasonal power spectrum was not well represented by a Markov process. Similarly, the EP pattern was also not well fitted by a Markov process.

a. Power spectra

The results of the power spectral analysis suggest that for intraseasonal periods (2–90 days) each (except for the atmospheric ENSO and EP patterns) of the above teleconnections patterns are well described by a Markov process. For interannual periods (2–20 yr), only the PNA showed a spectral peak (near 4 yr), which exceeded the 95% a posteriori confidence level.

b. Characteristic timescale

As stated above, the e -folding timescale for most of the teleconnection patterns was found to be on the order of 10 days. Thus, all of the above teleconnections are fundamentally short timescale processes. To illustrate these short timescale characteristics, we present an example showing the daily PNA PC time series during a particular winter season when the seasonally averaged PNA PC time series was strongly positive (see Fig. 5). As can be seen, the PNA PC time series is indeed dominated by numerous high-frequency fluctuations. The same behavior is also found for all the teleconnection patterns. The PC time series in Fig. 5 also illustrates the property that those winter seasons with a large time-averaged amplitude for a particular teleconnection pattern are characterized by high-frequency fluctuations with a preference for one particular sign. This suggests that the excitation mechanism for one sign of an anomaly must be taking place more frequently than that for the opposite sign anomaly during that particular winter. As an example, if short-term fluctuations in the positive (negative) PNA PC time series are excited by positive (negative) short-term tropical convective anomalies, it may be that a strong seasonal mean PNA anomaly is characterized by a preponderance of short-term convective anomalies of one particular sign.

The shortness of these timescales has important implications for the methodology adopted for examining various anomalies. This is because the calculation of monthly and seasonally averaged anomalies, as is done in most other studies, actually represents a temporal

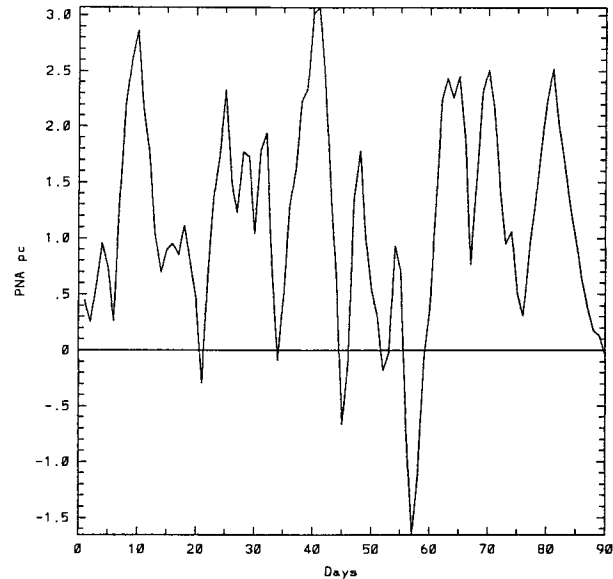


FIG. 5. The PNA PC time series for the 1986/87 winter.

averaging over many shorter timescale fluctuations. Such time averaging is beneficial, of course, if one's aim is to increase the signal-to-noise ratio in the data. In contrast, if one's goal is to improve our understanding of the fundamental dynamics of the growth and decay of teleconnection patterns, diagnostic analyses that focus on daily data should be very beneficial. Furthermore, the shortness of these timescales also implies that the physical processes that excite each teleconnection pattern must take place over a time period confined to several days. Consistent with this result, Cash and Lee (2000) find that a linear stochastic model forced by Gaussian white noise successfully captures the temporal evolution of the PNA.

These ideas can be succinctly illustrated by taking the time average of (1), the equation for a Markov process, that is, $\bar{x}_t = \alpha \bar{x}_{t-1} + \bar{F}_t$. Recall that x_t corresponds to the PC time series. In this equation, the overbar denotes a time average, which we apply to a time period over which a particular PC has a large amplitude of one sign, such as the time period shown in Fig. 5 for the PNA. If we are to relate this equation to the PNA (recall that the PC time series for the PNA is well described by a Markov process), then x_t corresponds to the amplitude of the PNA, and F_t the forcing, for example, anomalous tropical diabatic heating. Since we are applying this time average to a period of time over which a particular PC has a large amplitude, we assume that $\bar{x}_t = \bar{x}_{t-1}$, which leads to $(1 - \alpha)\bar{x}_t = \bar{F}_t$. Because of the short timescales of the teleconnections presented in this study, this indicates that teleconnections or anomalies in time-averaged data, for example, monthly or seasonally averaged data, represent the time-averaged response to time-average forcing, where both the response and forcing fluctuate rapidly in time. Thus,

monthly and seasonally averaged teleconnections should not be interpreted as corresponding to a steady, that is, time-independent, response to steady forcing, as might be implied from a time average.

c. *Climate noise*

The fact that most of the PC time series are well described as Markov processes directed us to investigate whether the interannual variability of these patterns arises from climate noise, that is, variability resulting from statistical sampling fluctuations. To address this question, we first specified a null hypothesis that the observed interannual variance is equal to that for a Markov process, and then evaluated statistical significance with χ^2 statistics. It was found that the interannual variance for the PNA PC time series exceeded the 95% confidence level. For the NAO, the interannual variance was found to be about halfway between that for the null hypothesis and the 95% confidence level. Such a value did not give sufficient confidence to make a strong statement about climate noise and the NAO. The interannual variance for the WP pattern, on the other hand, was close to that for the null hypothesis, which suggests that the interannual variability of this particular pattern can be attributed entirely to climate noise. The climate noise properties of the EA, EA/WR, and SCA patterns were also examined. It was found that interannual variance of the EA pattern exceeded the 95% confidence level, whereas that for the latter two patterns was fully within the range expected for climate noise.

The climate noise calculations also showed that the signal-to-noise ratio for the NAO was much smaller than that for the PNA, even though their interannual variances were very similar. These differences can in part be attributed to the longer timescale of the NAO. This is because a longer timescale, or equivalently a larger period at which the red noise spectrum becomes white, results in a greater interannual variance (Nitsche 1996).

d. *NAO, PNA, ENSO, and climate change*

The results of this study allow us to offer an explanation as to why it is that the NAO and PNA are the dominant patterns on interannual timescales. This is an interesting question because the fractional variance of the first several daily REOFs are all rather similar. For the NAO, it is likely because of its longer 9.5-day timescale. As stated above, the contribution of climate noise toward the interannual variance increases with a longer timescale. In contrast, the PNA likely attains its large interannual variance because of "external forcing," as suggested by the climate noise test. This external forcing is most likely associated with tropical Pacific SST anomalies, as shown in numerous observational and modeling studies.

Further insight into atmospheric interannual variability was obtained from a multiple regression calcu-

lation involving various PC time series and the Niño-3.4 index. The results of this calculation suggest that the atmospheric response to ENSO can be interpreted as a superposition of the atmospheric ENSO pattern, PNA and WP teleconnection patterns, with the contribution from the atmospheric ENSO pattern being dominant. This suggests that the atmospheric ENSO pattern is a much more robust response to ENSO forcing than the other patterns. Presumably, this is because on interannual timescales the atmospheric ENSO pattern is primarily driven by tropical heating associated with ENSO, whereas the other patterns are forced by a number of different processes.

One result of this study was that the two reddest (largest e -folding timescale) modes were those associated with the NAO and ENSO. This resembles the findings of von Storch (1999), who showed that the two reddest modes in a coupled general circulation model were associated with a tropical mode and a midlatitude mode, both exhibiting strong zonally symmetric characteristics. Their tropical mode was found to be related to the global relative angular momentum, a quantity highly correlated with ENSO (e.g., Chao 1988; Rosen et al. 1984), and their midlatitude mode showed characteristics extremely similar to the observed annular mode (Thompson and Wallace 1998, 2000a,b) and the observed zonal index (e.g., Feldstein and Lee 1998). For the Northern Hemisphere winter, the latter quantity is often considered to be the zonal average of both the NAO and the "annular mode" (Wallace 2000), also known as the Arctic oscillation (e.g., Thompson and Wallace 1998). In fact, by combining the results of this study with those of the zonal index study of Feldstein (2000) and with calculations of the spectral properties of the annular mode (based on sea level pressure; not shown), it is found that the e -folding timescale increases as the anomaly becomes increasing zonally symmetric. For example, the e -folding timescale for the NAO was shown in this study to be 9.5 days, for the more zonally symmetric Northern Hemisphere annular mode our calculations find a value of 10.6 days, and for the Northern Hemisphere zonal index, a timescale of 18 days is found (Feldstein 2000).

The findings of this study suggest a new avenue for improving our understanding, and perhaps predication of the teleconnection patterns. This involves an investigation of the life cycle of the teleconnection patterns, with an emphasis on the dynamical processes associated with their excitation, maintenance, and decay. Such a study is presently being undertaken by the author.

Acknowledgments. This research was supported by the National Science Foundation through Grant ATM-9712834. I would like to thank Drs. Sukyoung Lee and Saravanan for their beneficial discussions, and Mr. Henry Norwood and Dr. Mike Wallace for their helpful comments on this manuscript. Also, I would like to

thank the NOAA Climate Diagnostics Center for providing me with the NCEP–NCAR reanalysis dataset.

REFERENCES

- Barnston, A. G., and R. E. Livezey, 1987: Classification, seasonality, and persistence of low-frequency atmospheric circulation patterns. *Mon. Wea. Rev.*, **115**, 1083–1126.
- Cash, B. A., and S. Lee, 2000: Observed nonmodal growth of the Pacific–North American teleconnection pattern. *J. Climate*, in press.
- Chao, B. F., 1988: Correlation of interannual length-of-day variation with El Niño/Southern Oscillation, 1972–1986. *J. Geophys. Res.*, **93**, 7709–7715.
- Chatfield, C., 1989: *The Analysis of Time Series: An Introduction*. Chapman and Hall, 241 pp.
- Dole, R. M., 1986: Persistent anomalies of the extratropical Northern Hemisphere wintertime circulation: Structure. *Mon. Wea. Rev.*, **114**, 178–207.
- Feldstein, S. B., 2000: Is interannual zonal mean flow variability simply climate noise? *J. Climate*, **13**, 2356–2362.
- , and W. A. Robinson, 1994: Comments on ‘Spatial structure of ultra-low frequency variability of the flow in a simple atmospheric circulation model.’ *Quart. J. Roy. Meteor. Soc.*, **120**, 739–745.
- , and S. Lee, 1998: Is the atmospheric zonal index driven by an eddy feedback? *J. Atmos. Sci.*, **55**, 3077–3086.
- Horel, J. D., and J. M. Wallace, 1981: Planetary-scale atmospheric phenomena associated with the Southern Oscillation. *Mon. Wea. Rev.*, **109**, 813–829.
- Hurrell, J. W., and H. van Loon, 1997: Decadal variations in climate associated with the North Atlantic oscillation. *Climate Change*, **36**, 301–326.
- Kestin, T. S., D. J. Karoly, J.-I. Yano, and N. A. Rayner, 1998: Time-frequency variability of ENSO and stochastic simulations. *J. Climate*, **11**, 2258–2272.
- Leith, C. E., 1973: The standard error of time-averaged estimates of climatic means. *J. Appl. Meteor.*, **12**, 1066–1069.
- Madden, R. A., 1976: Estimates of the natural variability of time-averaged sea-level pressure. *Mon. Wea. Rev.*, **104**, 942–952.
- , and D. J. Shea, 1978: Estimates of the natural variability of time-averaged temperatures over the United States. *Mon. Wea. Rev.*, **106**, 1695–1703.
- Mo, K. C., and R. E. Livezey, 1986: Tropical–extratropical geopotential height teleconnections during the Northern Hemisphere winter. *Mon. Wea. Rev.*, **114**, 2488–2515.
- Nitsche, G., 1996: Some aspects of planetary-scale atmospheric variability in a low-resolution general circulation model. Ph.D. thesis, University of Washington, 208 pp. [Available from Department of Atmospheric Sciences, University of Washington, Seattle, WA 98195-7940.]
- Panofsky, H. A., and G. W. Brier, 1968: *Some Applications of Statistics to Meteorology*. Pennsylvania State University Press, 224 pp.
- Rosen, R. D., D. A. Salstein, T. M. Eubanks, J. O. Dickey, and J. A. Steppe, 1984: An El Niño signal in atmospheric angular momentum and Earth rotation. *Science*, **225**, 411–414.
- Thompson, D. W. J., and J. M. Wallace, 1998: The Arctic Oscillation signature in the wintertime geopotential height temperature fields. *Geophys. Res. Lett.*, **25**, 1297–1300.
- , and —, 2000a: Annular modes in the extratropical circulation. Part I: Month-to-month variability. *J. Climate*, **13**, 1000–1016.
- , and —, 2000b: Annular modes in the extratropical circulation. Part II: Trends. *J. Climate*, **13**, 1018–1036.
- Trenberth, K. E., 1984: Some effects of finite sample size and persistence on meteorological statistics. Part II: Potential predictability. *Mon. Wea. Rev.*, **112**, 2369–2379.
- , 1985: Potential predictability of geopotential heights over the Southern Hemisphere. *Mon. Wea. Rev.*, **113**, 54–64.
- von Storch, J.-S., 1999: The reddest atmospheric modes and the forcings of the spectra of these modes. *J. Atmos. Sci.*, **56**, 1614–1626.
- Wallace, J. M., 2000: North Atlantic oscillation/annular mode: Two paradigms—one phenomenon. *Quart. J. Roy. Meteor. Soc.*, **126**, 791–804.
- , and D. S. Gutzler, 1981: Teleconnections in the geopotential height field during the Northern Hemisphere winter. *Mon. Wea. Rev.*, **109**, 784–812.
- Wunsch, C., 1999: The interpretation of short climate records, with comments on the North Atlantic and Southern Oscillations. *Bull. Amer. Meteor. Soc.*, **80**, 245–255.
- Zhang, X., J. Shiang, and A. Shabbar, 1998: Modes of interannual and interdecadal variability of Pacific SST. *J. Climate*, **11**, 2556–2569.
- Zhang, Y., J. M. Wallace, and N. Iwasaka, 1996: Is climate variability over the North Pacific a linear response to ENSO? *J. Climate*, **9**, 1468–1478.